

The Blue Straggler population in the globular cluster M53 (NGC5024): a combined HST, LBT, CFHT study ¹

G. Beccari², B.Lanzoni², F.R. Ferraro², L.Pulone³, M.Bellazzini⁴, F.Fusi Pecci⁴, R.T.Rood⁵,
E.Giallongo³, R.Ragazzoni⁶, A.Grazian³, A.Baruffolo⁶, N.Bouche⁷, P.Buschkamp⁷, C.De
Santis³, E.Diolaiti⁴, A.Di Paola³, J.Farinato⁶, A.Fontana³, S.Gallozzi³, F.Gasparo⁸,
G.Gentile⁶, F.Pasian⁸, F.Pedichini³, R.Smareglia⁸, R.Speziali³, V.Testa³, E.Vernet⁹

ABSTRACT

We used a proper combination of multiband high-resolution and wide field multi-wavelength observations collected at three different telescopes (HST, LBT and CFHT) to probe Blue Straggler Star (BSS) populations in the globular cluster M53. Almost 200 BSS have been identified over the entire cluster extension. The radial distribution of these stars has been found to be bimodal (similarly to that of several other clusters) with a prominent dip at $\sim 60''$ ($\sim 2r_c$) from the cluster center. This value turns out to be a factor of two smaller than the radius of avoidance (r_{avoid} , the radius within which all the stars of $\sim 1.2 M_\odot$ have sunk to the core because of dynamical friction effects in an Hubble time). While in most of the clusters with a bimodal BSS radial distribution, r_{avoid} has been found to be located in the region of the observed minimum, this is the second case (after NGC6388) where this discrepancy is noted. This evidence suggests that in a few clusters the dynamical friction seems to be somehow less efficient than expected.

We have also used this data base to construct the radial star density profile of the cluster: this is the most extended and accurate radial profile ever published

²Dipartimento di Astronomia, Università di Bologna, via Ranzani 1, 40127, Bologna, Italy

³INAF, Osservatorio Astronomico di Roma, Via Frascati 33, I-00040, Monteporzio, Italy

⁴INAF-Osservatorio Astronomico di Bologna, via Ranzani 1, 40127, Bologna, Italy

⁵Astronomy Department, University of Virginia, Charlottesville, VA, 22903, rtr@virginia.edu

⁶INAF, Osservatorio Astronomico di Padova, Vicolo dell'Osservatorio, 5, I-35122 Padova, Italy

⁷Max-Planck-Institut für extraterrestrische Physik (MPE), Giessenbachstr.1, 85748 Garching, Germany.

⁸INAF, Osservatorio Astronomico di Trieste, Via G.B. Tiepolo 11, I-34131 Trieste, Italy

⁹INAF, Osservatorio Astronomico di Arcetri, Largo E. Fermi 5, I-50125, Firenze, Italy

for this cluster, including detailed star counts in the very inner region. The star density profile is reproduced by a standard King Model with an extended core ($\sim 25''$) and a modest value of the concentration parameter ($c = 1.58$). A deviation from the model is noted in the most external region of the cluster (at $r > 6.5'$ from the center). This feature needs to be further investigated in order to address the possible presence of a tidal tail in this cluster.

Subject headings: Galaxy: Globular Clusters — Individual: Messier Number: M53 — Stars: evolution, blue stragglers

1. Introduction

Globular Clusters (GCs) are ideal astrophysical laboratories for studying the evolution of both single stars and binary systems. In particular, the evolution and the dynamical interactions of binaries in high-density environments can generate objects (like Blue Straggler Stars, X-ray binaries, millisecond pulsars, etc.) that cannot be explained by standard stellar evolution. In this respect the most common exotic objects are the so-called Blue Straggler Stars (BSS). They are defined as those stars brighter and bluer (hotter) than the Main Sequence TurnOff (MS-TO), lying along an extrapolation of the MS. BSS are more massive than the normal MS stars (Shara et al. 1997), thus indicating that some processes which increase the initial mass of single stars must be at work. These could be related either to mass-transfer (MT) or merging processes between members of primordial binaries (PB-BSS), which mainly evolve in isolation in low density environment, or the merger of two single or binary stars driven by stellar collisions (COL-BSS), which are particularly efficient in high density regions. As shown by Ferraro et al. (2003), the two formation channels can have comparable efficiency in producing BSS in their respective typical environment (see the case of M80 and NGC288, Ferraro et al. 1999, Bellazzini et al. 2002). Moreover, these formation mechanisms could

¹Based on observations with the NASA/ESA HST, obtained at the Space Telescope Science Institute, which is operated by AURA, Inc., under NASA contract NAS5-26555. Also based on data acquired using the Large Binocular Telescope (LBT). The LBT is an international collaboration among institutions in the United States, Italy and Germany. LBT Corporation partners are: The University of Arizona on behalf of the Arizona university system; Istituto Nazionale di Astrofisica, Italy; LBT Beteiligungsgesellschaft, Germany, representing the Max-Planck Society, the Astrophysical Institute Potsdam, and Heidelberg University; The Ohio State University, and The Research Corporation, on behalf of The University of Notre Dame, University of Minnesota and University of Virginia. This research used the facilities of the Canadian Astronomy Data Centre operated by the National Research Council of Canada with the support of the Canadian Space Agency.

also act simultaneously within the same cluster, with efficiencies that depend on the radial regions, corresponding to widely different stellar densities. This hypothesis was suggested for the first time by Ferraro et al. (1993, 1997; hereafter F97): by using a proper combination of high-resolution and wide-field observations they studied the projected BSS radial distribution of the GC M3 over the entire cluster extension. The distribution turned out to be bimodal: it reaches the maximum at the center of the cluster, shows a clear-cut dip in the intermediate region (at $4r_c < r < 8r_c$), and rises again in the outer region (out to $r \sim 14r_c$). While the bimodality detected in M3 was considered for years to be *peculiar*, the most recent results demonstrated that this is not the case. The same observational strategy adopted by F97 in M3 has been applied to a number of other Galactic GCs, to study the BSS radial distribution over the entire cluster extension. Bimodal distributions with an external upturn have been detected in several cases: 47 Tuc (Ferraro et al. 2004), NGC 6752 (Sabbi et al. 2004), M55 (Zaggia et al. 1997; Lanzoni et al. 2007a), M5 (Warren et al. 2006; Lanzoni et al. 2007b), NGC 6388 (Dalessandro et al. 2007) and NGC 5466 (Beccari et al. 2008, in preparation). Extensive dynamical simulations (Mapelli et al. 2006; Lanzoni et al. 2007a) have been performed: they suggest that the observed central peak is mainly due to COL-BSS formed in the core and/or PB-BSS sunk to the centre because of dynamical friction effects, while the *external* rising branch is made of PB-BSS evolving in isolation in the cluster outskirts.

Even though the number of the surveyed clusters is low, the bimodal radial distribution first found in M3 and originally thought to be *peculiar* appears instead to be the *natural* one. However, generalizations made from a small samples are dangerous. Indeed, a few exceptions are already known: the BSS population in the high density GC NGC 1904 turns out to be highly centrally segregated but it does not show any external upturn (Lanzoni et al. 2007c). Moreover the BSS population in the massive GCs ω Cen (Ferraro et al. 2006a) and NGC 2419 (Dalessandro et al., 2008) has a radial distribution completely indistinguishable from that of other “normal” cluster stars. This is the cleanest evidence that these GCs are not fully relaxed, even in the central regions, and it suggests that the observed BSS are the progeny of primordial binaries, whose radial distribution was not yet significantly altered by stellar collisions and by the dynamical evolution of the cluster.

An even deeper insight on the BSS formation mechanism can be obtained by means of spectroscopic surveys able to measure the BSS surface abundance patterns. Recently Ferraro et al. (2006b) discovered that a sub-population of BSS in 47 Tuc shows a significant depletion in the Carbon and Oxygen surface abundances, with respect to the dominant BSS population and the normal cluster stars. Since incomplete CNO-burning products are expected at the surface of PB-BSS (Sarna & de Greve 1996), while normal abundances are predicted for COL-BSS (Lombardi et al. 1995), this discovery represents the first detection of a chemical signature clearly pointing to the MT formation process for BSS in a GC. However,

further spectroscopical analysis of BSS in a large sample of GCs are necessary in order to statistically increase the significance of the results obtained for 47Tuc. Unfortunately, because of the hostile environmental conditions (high crowding conditions of the cores of GCs), such observations are quite difficult. On the other side, photometric surveys, easier to perform, will allow to determine how common bimodality is, and what are its consequences for the theories of BSS formation and cluster dynamics.

Here we present a multiband photometric study of the GC NGC 5024 (M53), performed through a proper combination of data obtained by using three different telescopes: the Hubble Space Telescope (HST), the Large Binocular Telescope (LBT) and the Canada-France-Hawaii Telescope (CFHT). This large data-set allow us to resolve, for the first time, the stellar populations of this cluster from the very central regions out to a radius of 0.5 degree (~ 155 pc, assuming a distance from the Sun of 17.8 Kpc from Harris 1996) from the center. In Section 2 we present the observation and data reduction strategy. In Section 3 we describe the homogenization of the sample through accurate astrometry and photometric calibration. In section 4 we show the observed radial density profile of the cluster and the comparison with King models. Finally, in Section 6 we study the BSS radial distribution of the cluster.

2. Observations and data reduction

The photometric data used here consist of two main data sets. The *high resolution sample* consists of a set of HST images of the core region obtained with the Advanced Camera for Survey (ACS) through the F606W and F816W filters (GO-10775;P.I.: Sarajedini; see Table 1). All images were passed through the standard ACS/WFC reduction pipeline. Giving our interest in the brightest stars of the cluster and since stellar crowding is low in these images, we decided to perform aperture photometry using the SExtractor photometric package (Bertin et al. 1996), with an aperture radius of $0.15''$ (corresponding to a FWHM of 3 pixels). The source detection and the photometric analysis have been performed independently on each image. In the deepest exposure images only stars detected in three out five frames have been included in the final catalog. Finally, each ACS pointing has been corrected for geometric distortion using the prescriptions by Hack & Cox (2001) and a final catalogue was obtained. Since the central regions of the cluster are positioned in the very center of the ACS field of view (FoV), were also the gap between the two chips of the ACS is located, we decided to use a photometric catalogue of the cluster core obtained through the Planetary Camera (PC) chip of the Wide Field Planetary Camera 2 on board of HST.

This has been retrieved from the HST Snapshot published by Piotto et al. (2002)².

The *wide field sample* consists of deep multi-filter (U , B and V ; see Table 1) wide-field images, secured during the Science Demonstration Time (SDT) of LBC-Blue (Ragazzoni et al. 2006; Giallongo et al. 2008) mounted on the LBT, sited at Mount Graham, Arizona (Hill et al. 2006). The LBC is a wide-field imager which provides an effective $23' \times 23'$ FoV, sampled at 0.224 arcsec/pixel over four chips of 2048×4608 pixels each. LBC-Blue is optimized for the UV–blue wavelengths, from 320 to 500 nm, and is equipped with the U , B , V , g and r filters. The core of the cluster has been positioned in the central chip (namely #2) of the LBC-Blue CCD mosaic. Here we present only the photometric reduction of the shortest exposures (see Table 1). The photometry of the complete data-set, including the longest exposures, will be presented in a forthcoming paper (Beccari et al. 2008, in preparation). The raw LBC images were corrected for bias and flat field, and the overscan region was trimmed using a pipeline specifically developed for LBC image pre-reduction from LBC-team at Rome Astronomical Observatory³. The source detection and relative photometry was performed independently on each U , B and V image, using the PSF-fitting code DaoPHOTII/ALLSTAR (Stetson 1987, 1994).

In order to sample the entire extension of the cluster, additional archive g and r wide-field MEGACAM images were taken from the Canadian Astronomy Data Centre (CADC⁴). Mounted at CFHT (Hawaii), the wide-field imager MEGACAM (built by CEA, France), consists of 36 2048×4612 pixel CCDs (a total of 340 megapixels), fully covering a 1 degree \times 1 degree FoV with a resolution of 0.187 arcsecond/pixel. The data are preprocessed (removal of the instrumental signature) and calibrated (photometry and astrometry) by Elixir pipeline. Giving the very low crowding conditions of the external regions, we performed aperture photometry using SExtractor with an aperture radius of $0.9''$ (corresponding to a FWHM of 5 pixels). Each of the 36 chips was reduced separately, and we finally obtained a catalogue listing the relative positions and magnitudes of stars in common between the g and r data-set.

²The catalogue is available at web site <http://www.astro.unipd.it/globulars/>

³<http://lbc.oa-roma.inaf.it/>

⁴<http://www3.cadc-ccda.hia-ihp.nrc-cnrc.gc.ca/cadc/>

3. Homogenization of the catalogues: Astrometry and Photometric calibrations

In Figure 1 we show a map of the adopted data-sets. In order to properly combine the available catalogues is crucial to find a proper astrometric solution over the entire sampled area. For this purpose we used the same method largely employed and described in the literature (see for example Lanzoni et al. 2007a, and references therein). We used thousand stars in common with a SDSS catalogue⁵ covering an area of 1 square degree, centered on the cluster, in order to obtain an absolute astrometric solution for each of the 36 chips over the MEGACAM FoV, with a final global accuracy of $0.3''$ r.m.s. both in right ascension (α) and declination (δ); note that the WCS informations available in the FITS images processed by the Elixir pipeline are given with a global accuracy $\sigma > 0''.5$. The same technique applied to LBC-Blue sample gave an astrometric solution with similar accuracy, i.e. $\sigma < 0.3''$ r.m.s.. Considering that the very central regions of the cluster are not provided with standard astrometric stars, we used the stars in LBC-Blue catalogue as *secondary astrometric standards* for finding a good astrometric solution for the high-resolution sample. We thus obtained an astrometric solution for the stars in the core region with the same accuracy obtained in previous cases.

The different data sets were first calibrated in the respective photometric systems. The photometric calibration of the g and r magnitudes in the MEGACAM sample was performed using the stars in common with SDSS catalogue. In order to transform the instrumental B and V magnitudes of the LBC-Blue sample into the Johnson standard system we used the stars in common with a photometric catalogue previously published by Rey et al. (1998, hereafter R98). The most isolated and brightest stars in the ACS field have been used to link the aperture magnitudes at $0.5''$ to the instrumental ones, after normalizing for exposure time. Instrumental magnitudes have been transformed into the VEGAMAG system by using the photometric zero-points by Sirianni et al. (2005). Finally, the catalogue of the HST Snapshot is provided with the magnitudes both in the $F439W$ and $F555W$ flight system and in the standard Johnson B and V systems.

Appropriate photometric transformations were then applied to convert the g and $F606W$ into standard V Johnson. This allows us to use the V magnitudes as reference between all the data-sets. In Figure 2 and 3 we show the CMDs of the high-resolution (ACS, left panel; WFPC2/PC, right panel) and wide-field samples (LBC-Blue, left panel; MEGACAM, right panel) respectively.

⁵Available at web-site <http://cas.sdss.org/dr6/en/tools/search/radial.asp>

In order to perform the most complete and homogeneous sampling of the cluster, we decided to use the high-resolution dataset for the central area, the LBC-Blue catalog for the region out to a radius $r = 630''$ from the center, and the MEGACAM sample for $r > 630''$. Moreover, only stars in the magnitude range $16.5 < V < 21$ have been considered in the combined high resolution + wide-field catalogs. A completeness study performed over the ACS images in the considered magnitude range has shown that the completeness is larger than 90%. Moreover, we have verified that all the stars of the R98 catalogue lying in the region in common with our LBC-Blue dataset are recovered in the LBC-Blue sample. Hence, from Figure 3 of R98, we estimated a level of completeness greater than 80% for the LBC-Blue catalogue. Finally, by comparing star count density profiles in the region in common between the LBC-Blue and the MEGACAM data we verified that the two samples have the same level of completeness.

4. The cluster density profile

The extended data set collected for this cluster offered the possibility to compute its detailed radial star density profile, from the center, out to distances beyond the tidal radius ($r_t \simeq 22'$ from Harris 1996). Using the sample as previously defined (see also Figure 1) we have determined the projected density profile of M53 by direct star counts. Following the procedure already described in Lanzoni et al. (2007a), we have divided the entire sample into 27 concentric annuli, each split in an adequate number of sub-sectors (quadrants). The number of stars lying within each sub-sector was counted, and the star density was obtained by dividing these values by the corresponding sub-sector areas. The stellar density in each annulus was then obtained as the average of the sub-sector densities, and the standard deviation was estimated from the variance among the sub-sectors.

The radial density profile thus derived is plotted in Figures 4 and 5. Notice that from a radius $r \simeq 16.6'$ outwards, the statistical contamination of the background stars starts to dominate the stellar counts. The average of the two outermost surface density measures has been adopted as the background contribution (corresponding to $0.57 \text{ stars/arcmin}^{-2}$). Our profile is in excellent agreement with that published by Trager et al. (1995), in the region from $r = 0''$ to $r \simeq 550''$. In order to reproduce the observed profile, isotropic, single-mass King models have been computed. As shown in Figure 4, the best fit model (reduced $\chi^2 = 2.3$) is characterized by a core radius $r_c \simeq 25''$ and a concentration $c \simeq 1.6$. In Figure 5 (panel a) we show, for comparison, the King model with parameters $r_c \simeq 22''$ and $c \simeq 1.8$ adopted by Harris (1996). As apparent, the quality of the fit is significantly worse ($\chi^2 = 5.5$) than in the case of our best-fit model. As shown in panel b of Figure 5, a model

with lower concentration ($c = 1.45$) and larger core radius ($r_c = 26''$) best reproduces the inner portion of the observed profile. In fact, considering the region within a radius $r < 4.2'$, we have $\chi^2_{r < 4.2'} = 0.32$, while for the best fit model we have $\chi^2_{r < 4.2'} = 1$. However the low concentration model strongly disagrees with the observations in the outer regions, while the discrepancy is not statistically significant for the adopted best-fit model. Such a change of slope of the surface density profile might be the signature of the presence of tidally stripped stars (see Combes et al. 1999; Johnston et al. 1999; Leon et al. 2000, and references therein). This aspect need to be further investigate since, up to now, no evidence of tidal tail have been detected for M53.

5. The cluster population selection

In Figure 2 we show the population of BSS (open circles) and horizontal branch (HB; open triangles) stars selected in each data-set. Their number counts are reported in Table 2.

As largely discussed in the literature, in order to study the radial distribution of BSSs, one needs to compare their number counts as a function of radius to those of a population assumed to trace the overall radial density distribution of the cluster. For homogeneity with our previous works (see Lanzoni et al. 2007a, and references therein), we decided to use the Horizontal Branch (HB) stars as reference population. The BSS selection box was initially defined in the WFPC2/PC ($B, B - V$), ACS ($V, V - I$) and LBC-Blue ($B, B - V$) CMDs, as the region containing most of the BSSs in common with R98, who studied the BSS radial distribution within $\sim 9'$ from the cluster center. Then the BSSs thus identified in the LBC-Blue catalogue which are in common with the MEGACAM one, allowed us to properly define a selection box in the ($V, V - r$) plane. Giving the excellent quality of all the CMDs, the HB population is easily separable from the Red and Asymptotic Giant Branch sequences. Moreover, the SX Phoenicis and RRlyrae stars identified by comparing our catalogues with previously published works (Jeon et al. 2003; Clement et al. 2001, for the SX Phoenicis and RRlyrae, respectively), were included in the BSS and HB populations, respectively. All the populations thus selected in each data-set, are marked in Figure 2, and their number counts are reported in Table 2. Since at $r > 16.6'$ the stellar counts start to be dominated by background stars (see Section 4), in the following analysis we only consider the BSS and HB stars within this distance from the cluster center.

6. Results: the BSS radial distribution

The radial distribution of BSSs identified in M53 has been studied following the same procedure previously adopted for other clusters (see Lanzoni et al. 2007a, and references therein). In Figure 6, we compare the BSS cumulative radial distribution to that of HB stars. As can be seen, the behavior of the two distributions is not monotonic since the BSSs appear to be more concentrated than the HB stars in the central region and less concentrated in the outer region. This trend resembles that found for M3 by Ferraro et al. (1997). Following the Kolmogorov-Smirnov test (KS), there is a probability of 95% that the BSS population has a different radial distribution with respect to that of HB stars.

For a more quantitative analysis, the surveyed area has been divided in concentric annuli centered on the cluster center (from Harris 1996). We have chosen 7 concentric annuli (see Table 3), each containing a fairly similar number of HB stars. Then, we counted the number of BSSs (N_{BSS}) and HBs (N_{HB}), and we computed the N_{BSS}/N_{HB} ratio in each annulus. In the upper panel of Figure 7 we show the radial distribution of this ratio. It clearly shows a bimodality, with a high frequency of BSSs in the inner and outer regions, but a distinct dip in the intermediate region. The results for $r < 9'$ well agree with those obtained by R98. Then, thanks to the much larger extension of our data-set, the existence of an upturn of the BSS radial distribution in the most external regions is clearly apparent. The significance of the observed dip in the region $30'' < r < 80''$ can be assessed by noting that 50 BSS (instead of the 25 observed) would be needed in this region in order to flatten the distribution. From Poisson statistics alone, the observed number (25) thus represents a 5σ fluctuation from the expected value (50). An alternative possibility is that the BSS population is affected by a lower level of completeness than the HB one. In order to investigate this problem, we selected a population of Red Giant and Sub Giant Branch (RGB and SGB, respectively) stars in the same magnitude range as defined for the BSSs. In this case the KS test reveals that the cumulative radial distribution of the RGB+SGB population (dotted line in Figure 6) is different from that of BSS, with a 98.7% significance. By using this population as reference, we calculated the ratio between N_{BSS} and the number of RGB+SGB stars (simply N_{RGB}) in the same annuli as previously defined. As shown in the lower panel of Figure 7, the radial distribution of the specific frequency N_{BSS}/N_{RGB} shows exactly the same properties as that of N_{BSS}/N_{HB} .

As a further confirmation of this observational feature, we decided to study also the radial distribution of the BSS compared to HB stars normalized to the sampled luminosity. By defining N_{pop} the number of stars of a given population in a given ring, and L_{sample} the sampled light in that ring, the double normalized ratio (R_{pop}) in each annulus is (Ferraro et al.

1993)

$$R_{\text{pop}} = \frac{N_{\text{pop}}/N_{\text{pop}}^{\text{tot}}}{L_{\text{sample}}/L_{\text{sample}}^{\text{tot}}}$$

where $N_{\text{pop}}^{\text{tot}}$ and $L_{\text{sample}}^{\text{tot}}$ are the total sampled population and luminosity, respectively. The luminosity in each annulus has been calculated by summing up the luminosity of each sampled star (with $21 < V < 16.5$). The double normalized ratio of BSS and HB stars calculated in each annulus is reported in Table 3, and their radial distribution is plotted in Figure 8. As can be seen, the HB double normalized ratio remains essentially constant around unity over the surveyed area. This is in agreement with the fact that the fraction of HB (as of any post-MS) stars in each annulus strictly depends on the fraction of luminosity sampled in that annulus (see the relation in Renzini & Buzzoni 1986). In contrast, the BSS double normalized ratio reaches a maximum at the center of the cluster, decreases and reaches a minimum at $r \sim 1'$, and then rises again. This behavior fully confirms the trend shown in Figure 7 and suggests that dynamical events and/or different formation mechanisms shape the radial distribution of the BSSs in the cluster (see Mapelli et al. 2006).

As previously discussed, a bimodal radial distribution of BSSs like the one found here for M53 has been detected in several GCs studied with a similar observational strategy (e.g. M3, 47 Tuc, NGC6752, M5, M55; see references in Dalessandro et al. 2007). By using the best-fit King model presented in Section 4, with central density and velocity dispersion $\rho_0 = 2.2 \times 10^3 M_{\odot}/\text{pc}^3$ and $\sigma \sim 6.7 \text{ km s}^{-1}$, respectively (from McLaughlin & van der Marel 2005), and assuming 12 Gyr as the cluster age, we estimated the value of the radius of avoidance (r_{avoid}) from the dynamical friction time-scale formula (e.g., Mapelli et al. 2006). This is defined as the radius within which all the stars of $\sim 1.2 M_{\odot}$ (value that well represents the average mass of the BSSs) have already sunk to the core because of dynamical friction effects. For M53 we found a value of $r_{\text{avoid}} \simeq 4.6r_c$, that corresponds to $\simeq 115''$ by assuming $r_c = 25''$ and is marked with a vertical arrow in both panels of Figure 7. As apparent, this value is a factor of two larger than the observed minimum, which occurs at $\sim 2r_c$ from the cluster center. For the adopted central velocity dispersion⁶ and for BSS masses ranging between 1 and $1.5 M_{\odot}$, completely unrealistic cluster ages ($t < 4 \text{ Gyr}$) would be necessary in order to reconcile the value of r_{avoid} with the position of the observed minimum. However, if σ is underestimated by 50% (i.e., if $\sigma = 10 \text{ km/s}$), an agreement between the two quantities is found for $t \sim 10 - 12 \text{ Gyr}$ and $M_{\text{BSS}} = 1 - 1.2 M_{\odot}$. An observational measure of the central velocity dispersion of M53 and accurate dynamical simulations are therefore urgent in order to better understand the origin of the observed discrepancy.

⁶Note that the value listed by McLaughlin & van der Marel (2005) is not observed but derived from a dynamical King model.

Indeed, although our estimate of r_{avoid} is quite rough, it is interesting to note that in most of the clusters with a bimodal BSS radial distribution, r_{avoid} has been found to be located within the region of the observed minimum (see Dalessandro et al. 2007, and references therein). The main exception to this rule is the case of NGC6388, where Dalessandro et al. (2007) found that r_{avoid} is 3 times larger than the position of the observed minimum. The result presented here for M53 is similar to that of NGC6388 and it suggests that in a few clusters the dynamical friction seems to be somehow less efficient than expected. Which is the origin of this low efficiency? Could the history of each individual cluster play a role in this?

We also note that the value of r_{avoid} estimated for M53 is very similar to that found for M3 ($\sim 4.9 r_c$; Mapelli et al. 2006). Moreover, the two clusters seem to share some similarities: (1) the structural parameters (listed in Table 4) are quite similar; (2) the specific frequency N_{BSS}/N_{HB} within $20''$ from the cluster center is similar (0.51 ± 0.01 , 0.53 ± 0.01 for M53 and M3, respectively). In Figure 9 the radial distribution of N_{BSS}/N_{HB} for the two clusters is shown. As apparent, while the computed values of r_{avoid} turn out to be located at approximately the same distance in the two clusters, the location of the observed minimum of the distribution is sensibly different: in particular, in M53 the region where the dynamical friction has been efficient in segregating massive stars toward the cluster center is significantly more internal than in M3.

Hence, while the central value of the specific frequency suggest a similar overabundance of BSSs in the centre of the two clusters, the different location of the minimum of the distributions suggests that M53 is dynamically younger than M3 (i.e. that, for some reasons, the dynamical friction has been less efficient in M53). As shown in Mapelli et al. (2006), the central peak of the radial distribution of M3 is found to be mainly generated by COL-BSSs, while the external upturn is due to the presence of a genuine population of MT-BSS. While analogous conclusions might also apply to the case of M53, the origin of the diversity needs to be further investigated through detailed numerical simulations. We once more emphasize that the BSS radial distribution contains crucial information about the dynamical history and evolution of stellar systems.

We would thank the anonymous Referee for the rapid and useful comments. This research was supported by the Agenzia Spaziale Italiana (under contract ASI-INAF I/016/07/0) and by the Ministero dell’Istruzione dell’Università e della Ricerca. It is also part of the “*Progetti Strategici di Ateneo 2006*” granted by University of Bologna. The authors thank the LBT Science Demonstration Time (SDT) team for assembling and executing the SDT program. We also thank the LBC team and the LBTO staff for their kind assistance.

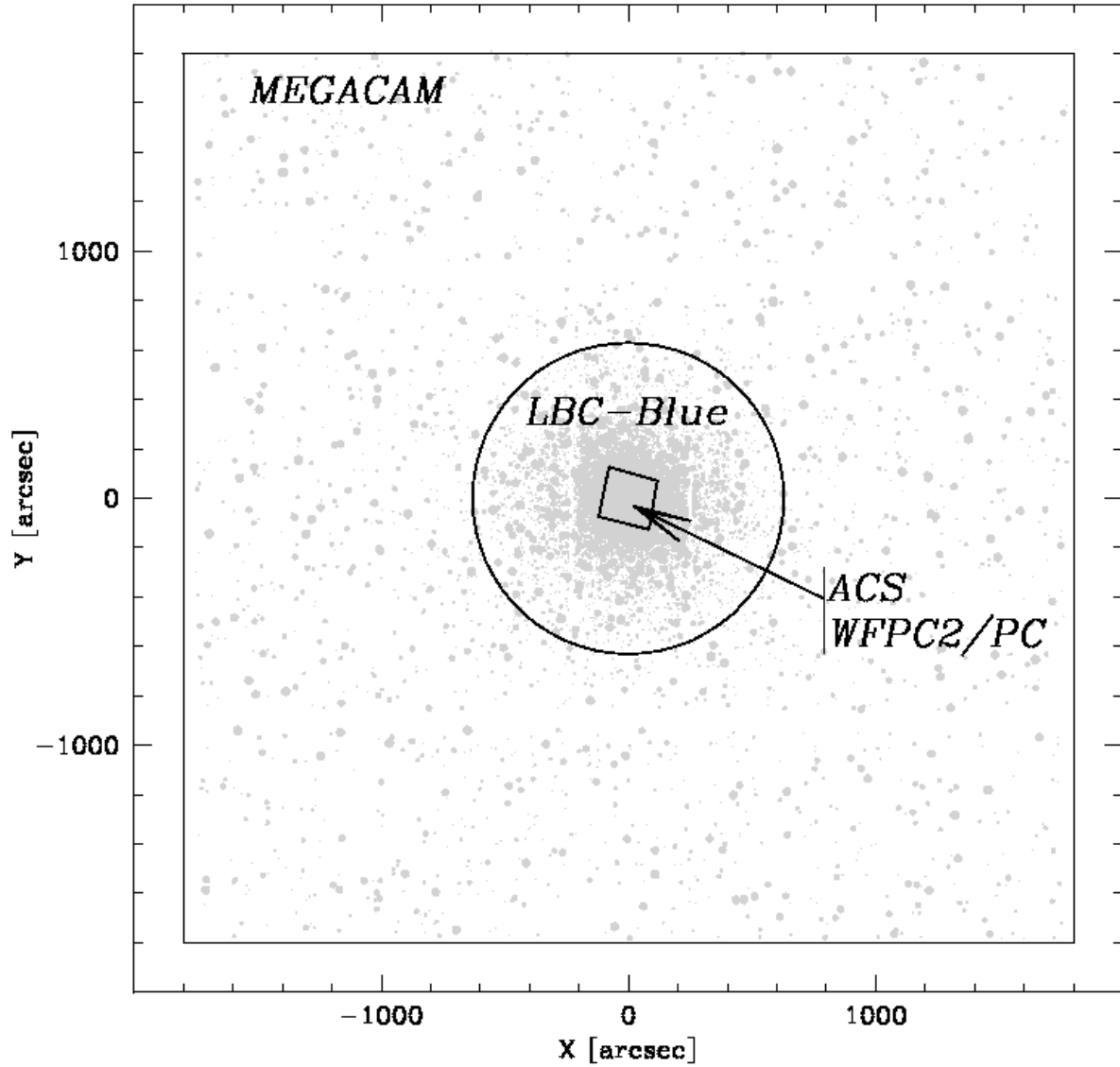


Fig. 1.— Map of the combined data-set used to sample the total radial extension of M53. The circle defines the cluster area probed by the LBC-Blue data, while the inner and outer squares correspond to the ACS and MEGACAM fields of view.

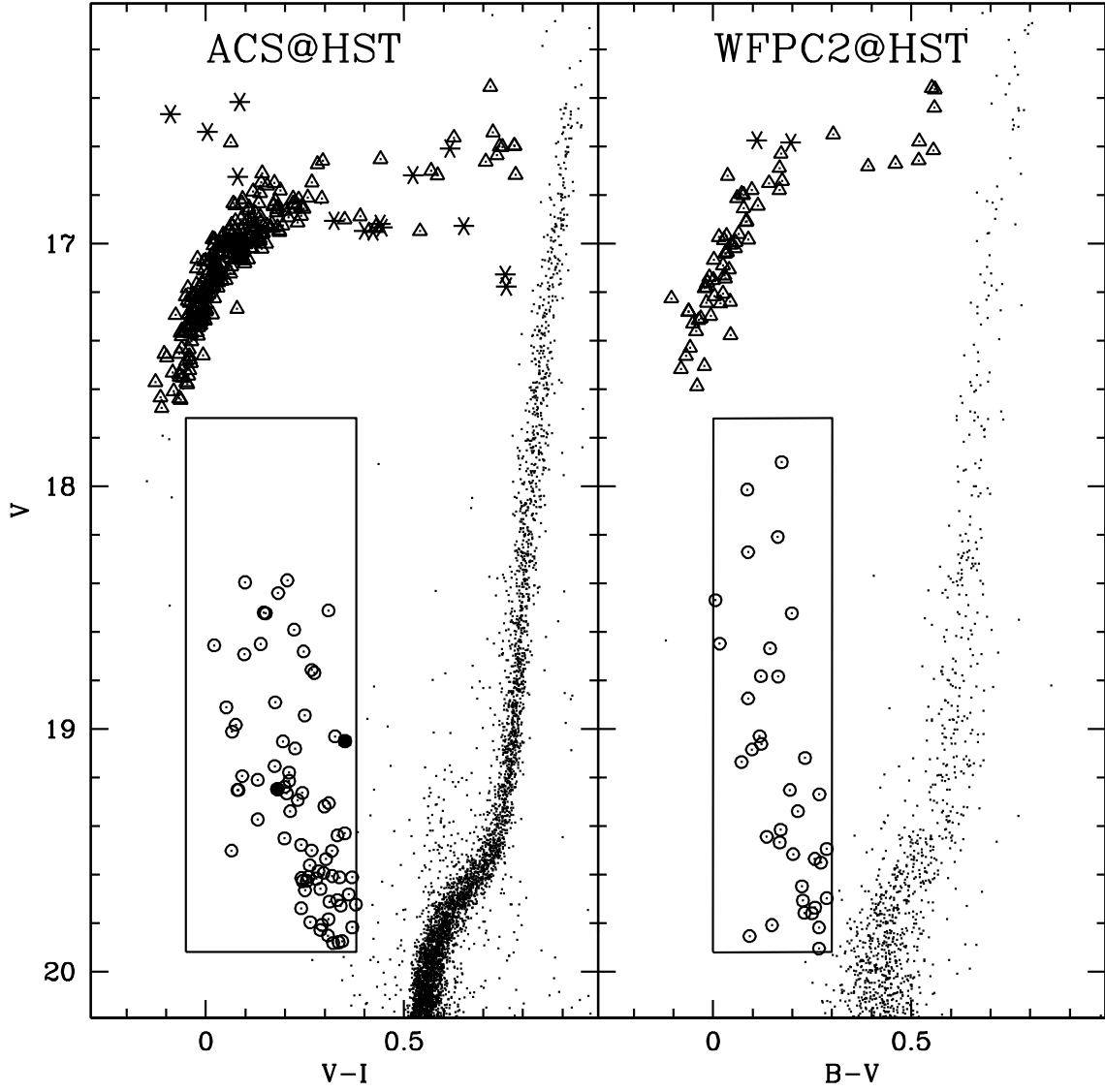


Fig. 2.— CMDs of the high resolution sample. Open circles mark the BSSs, filled circles the SX Phoenixis, open triangles the HB stars and asterisks the RR Lyrae stars.

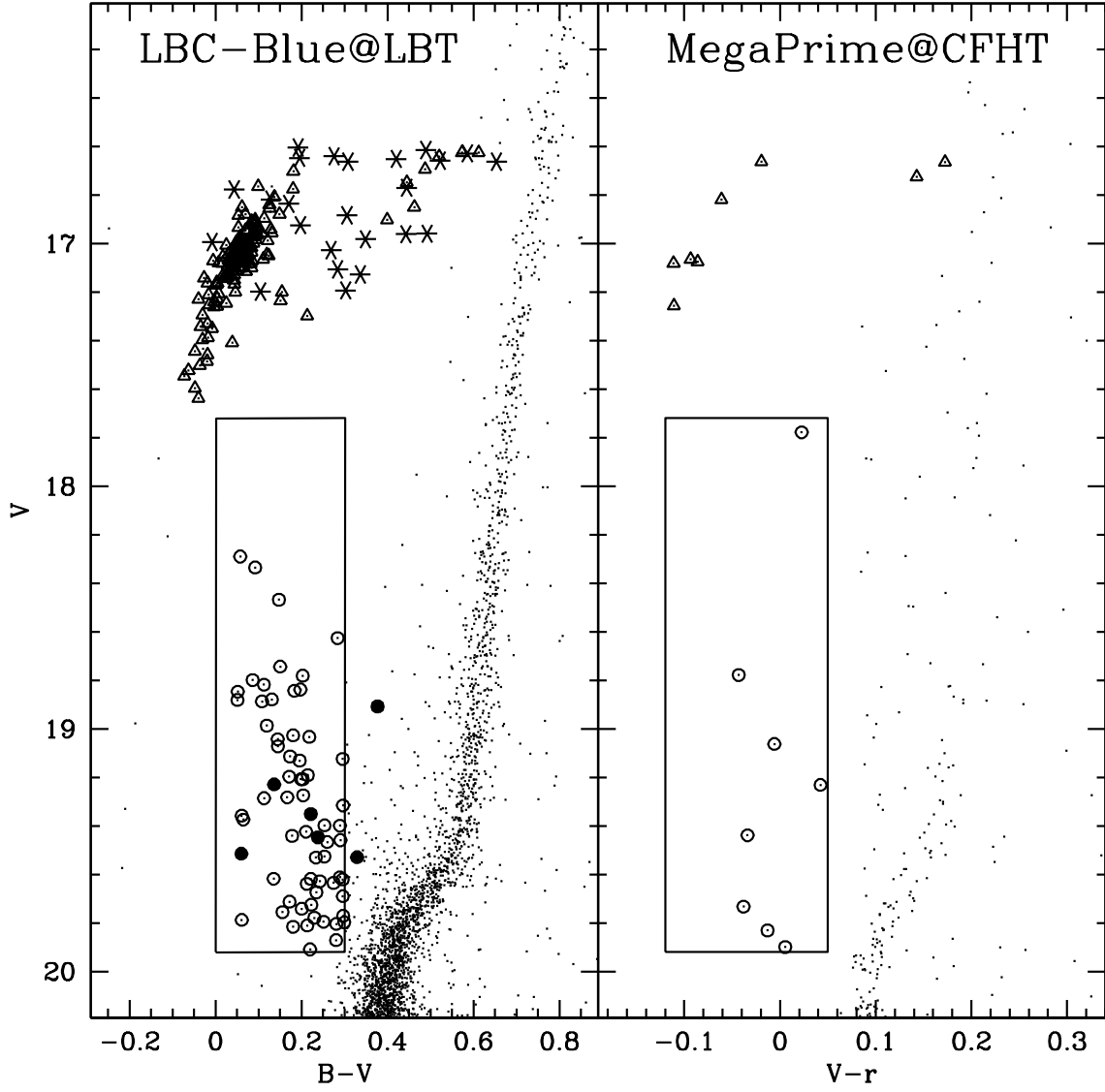


Fig. 3.— CMDs of the wide field sample. Symbols are the same as in Figure 2.

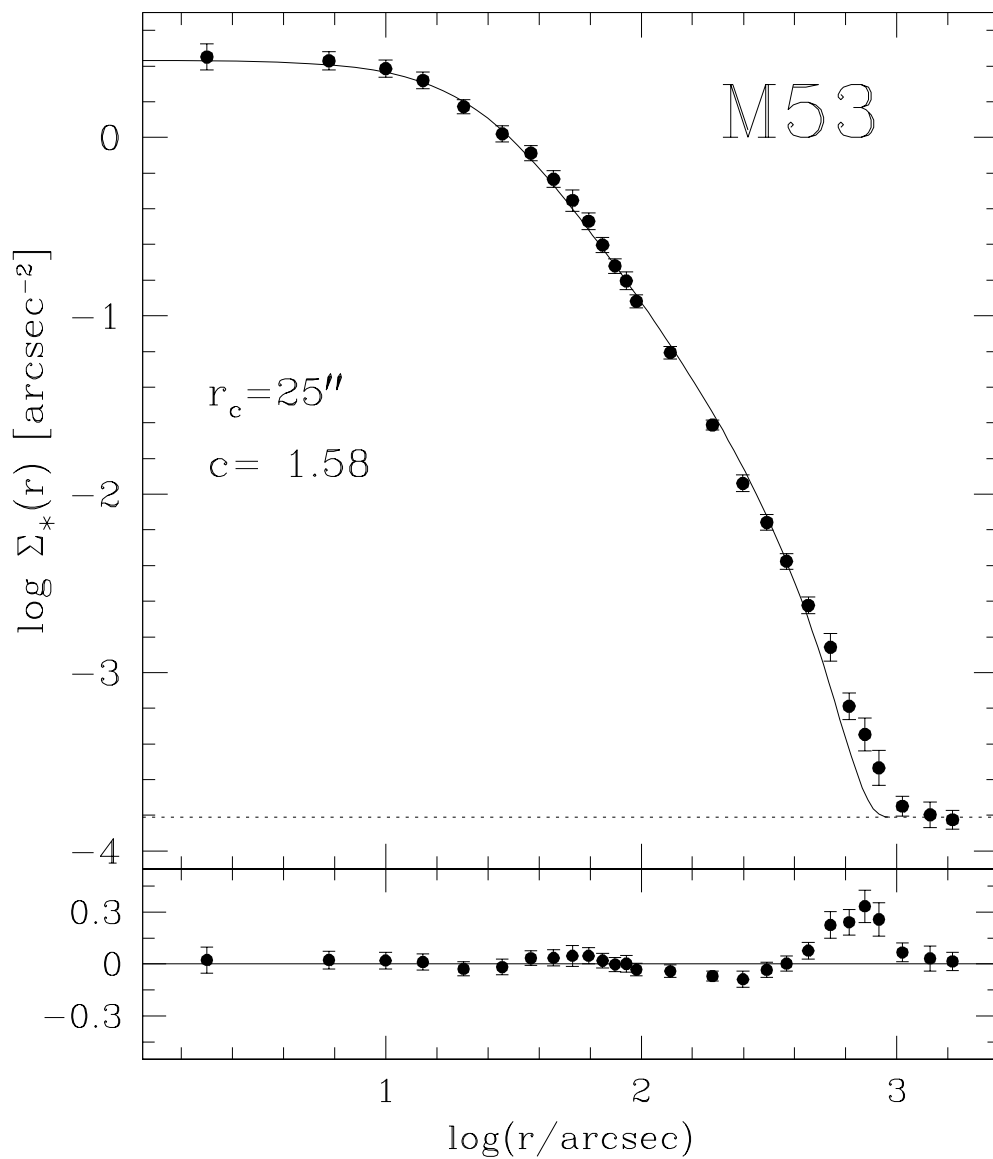


Fig. 4.— Observed surface density profile (filled circles and error bars) in units of number of stars per square arcseconds. The solid line is the King model ($c = 1.58$; $r_c = 25''$) that best fits the observed density profile over the entire cluster extension. A value of $0.54 \text{ stars/arcmin}^2$ is adopted as the field contamination density (dashed line). Notice that starting from a radius $r \gtrsim 16.6'$ field star counts become dominant.

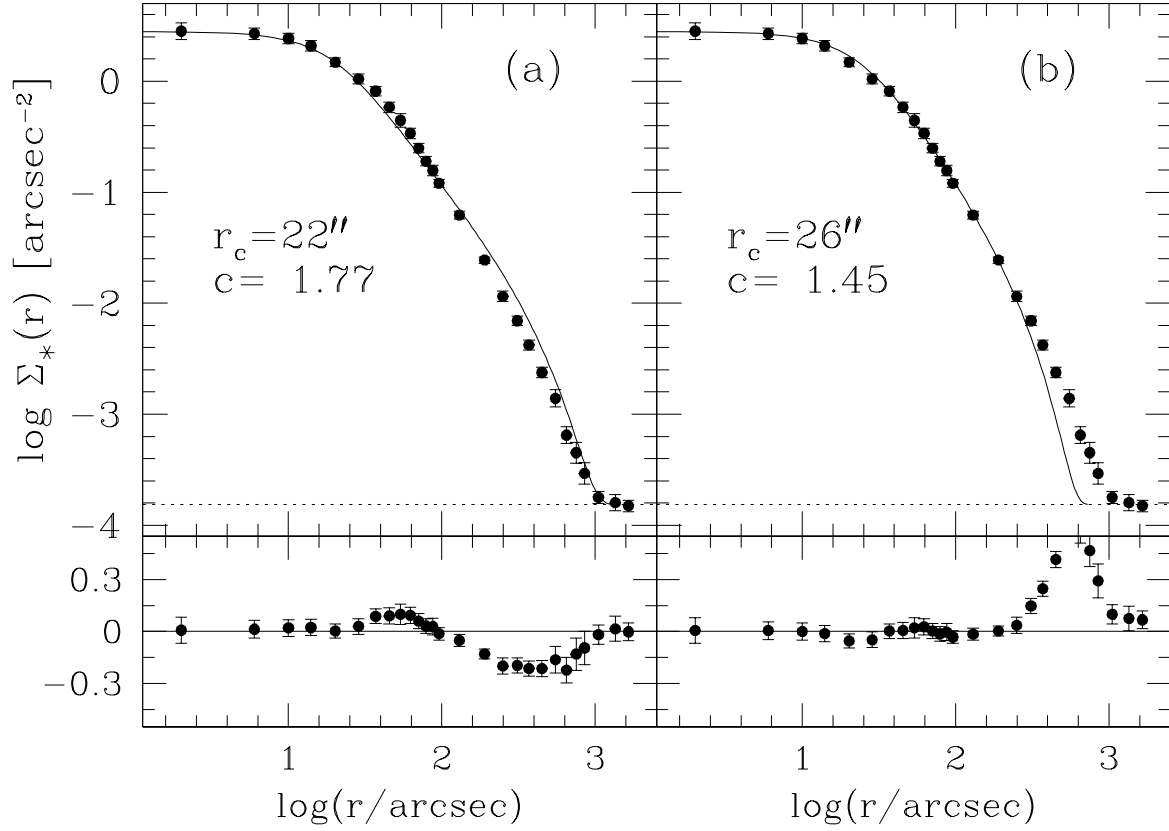


Fig. 5.— Observed surface density profile compared to the King models obtained using the values of r_c and c quoted by Harris (1996, panel *a*), and optimizing the fit in the central regions ($r < 4.2'$; panel *b*).

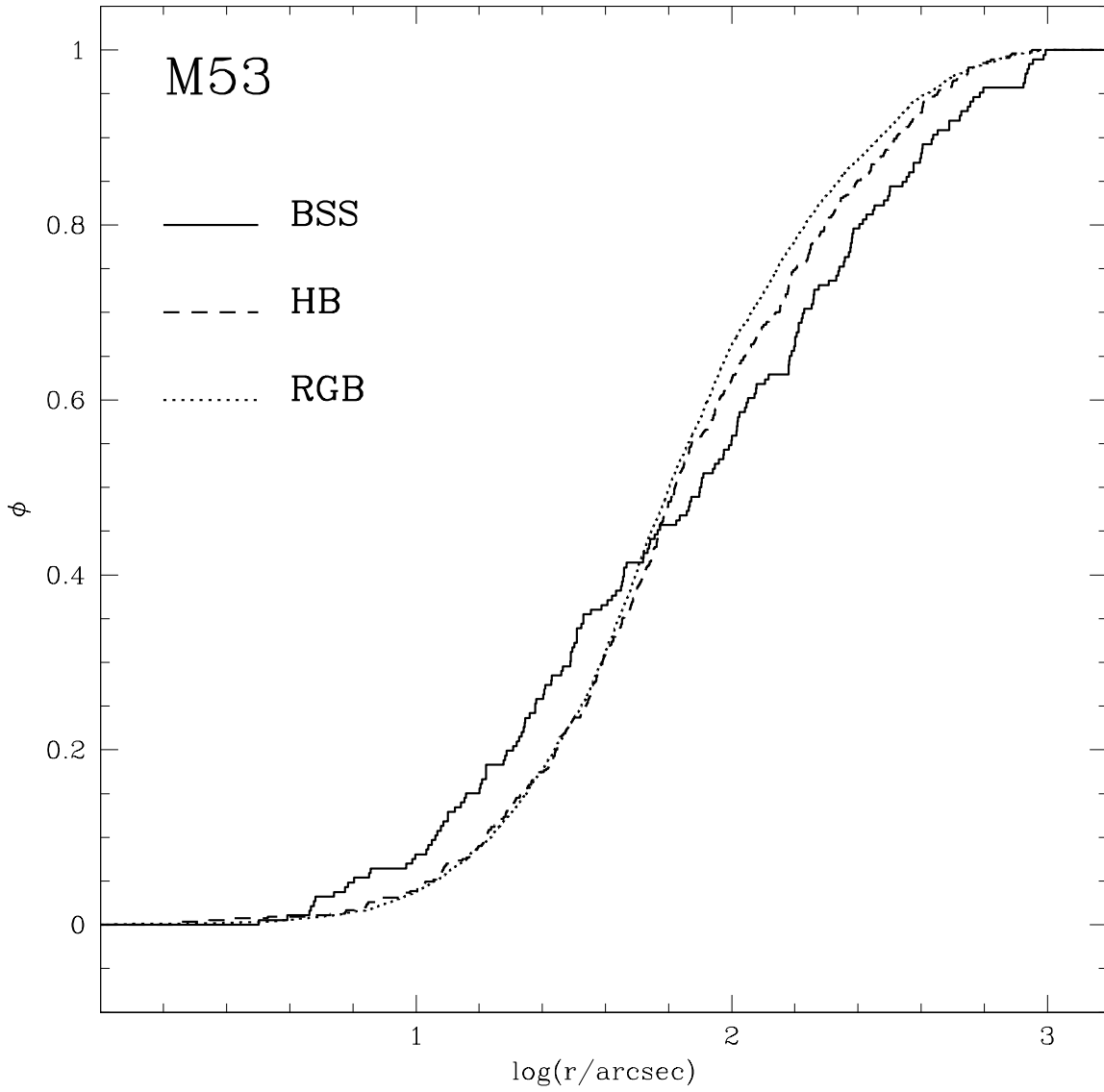


Fig. 6.— Cumulative radial distribution of BSSs (*solid line*), HB stars (*dashed line*) and RGB+SGB stars (*dotted line*), as a function of the projected distance from the cluster center.

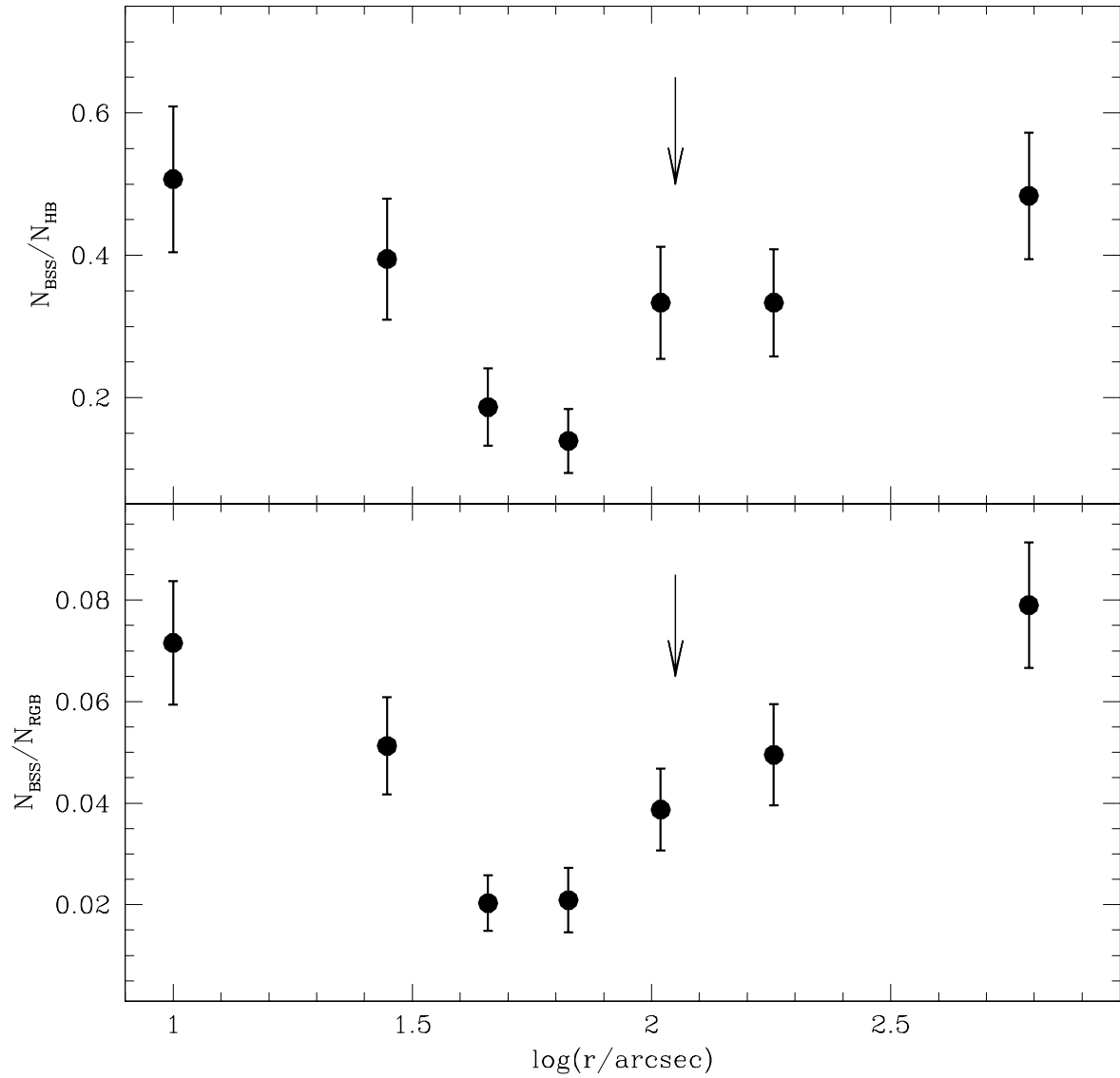


Fig. 7.— Relative frequency of BSSs with respect to HB (*upper panel*) and RGB+SGB stars (*lower panel*), plotted as a function of the distance from the cluster center. The vertical arrows represent the estimated position of the radius of avoidance of the cluster (see text for details).

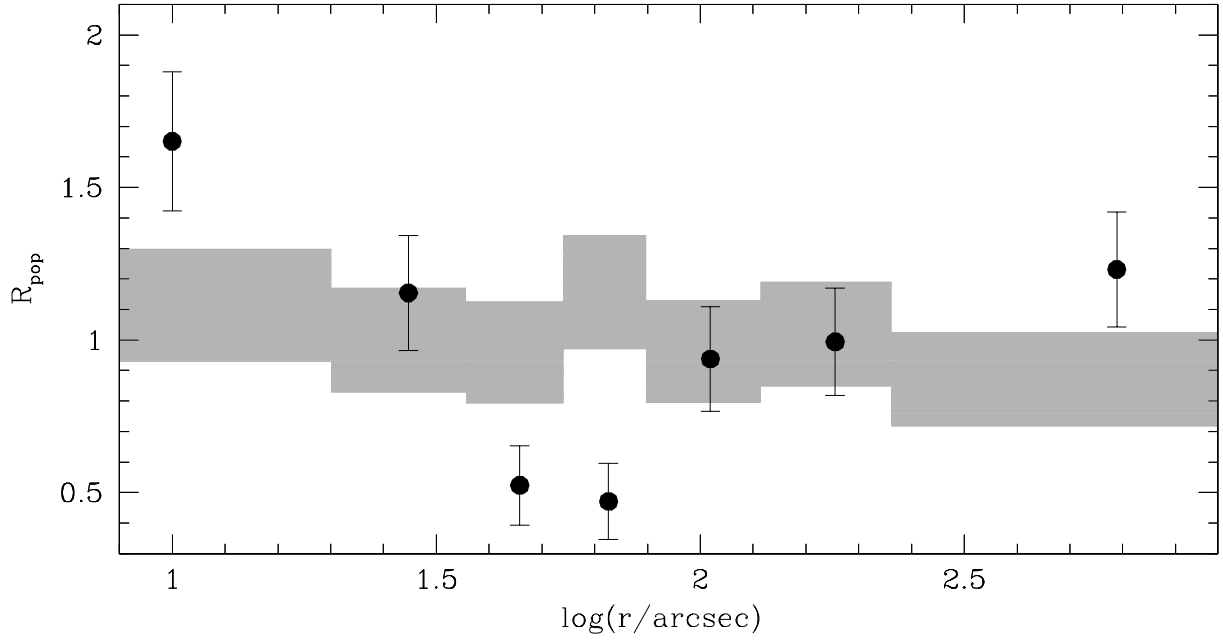


Fig. 8.— Double normalized ratio (see text) of BSSs (dots and error bars) and of HB stars (gray regions).

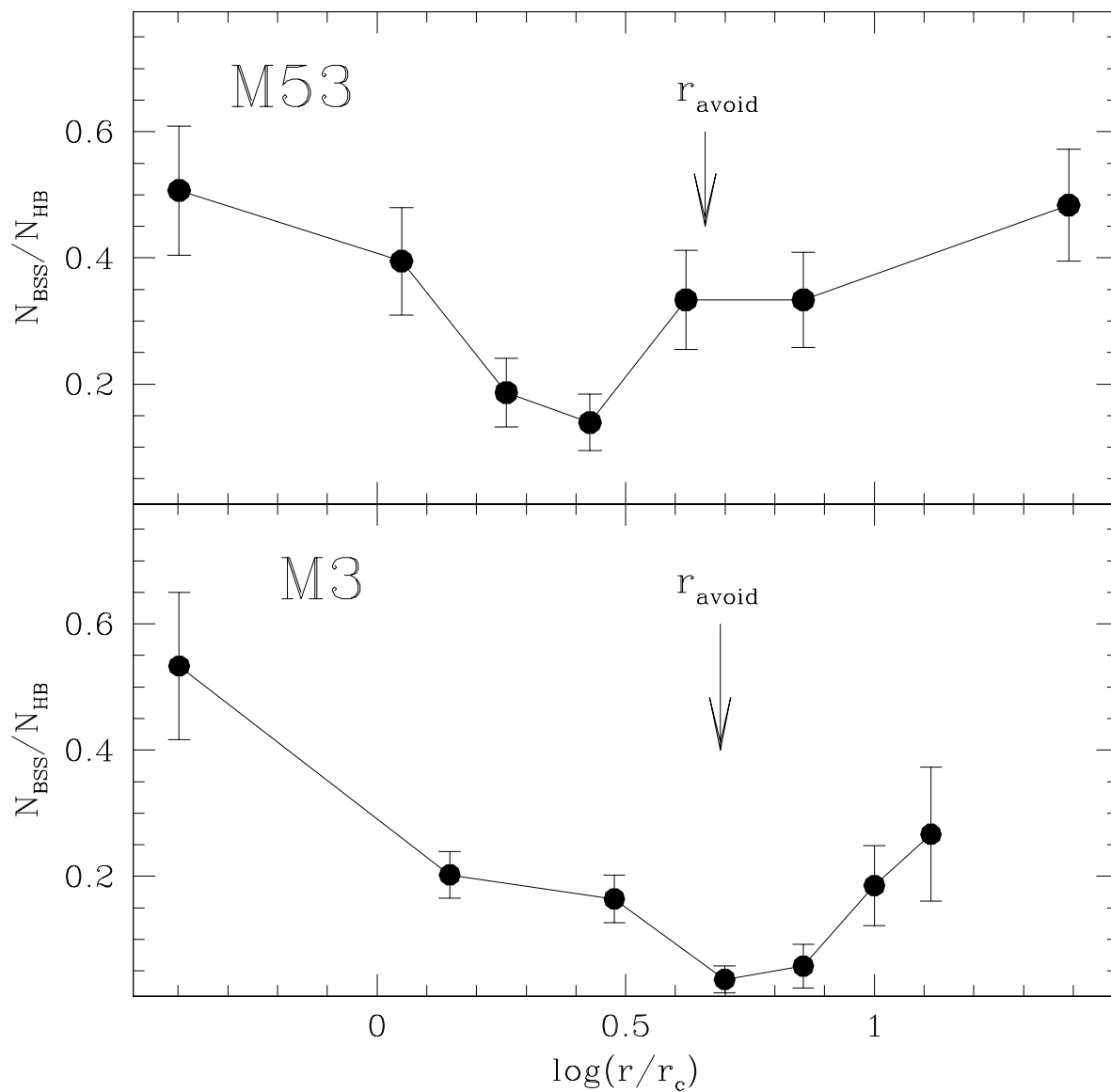


Fig. 9.— Relative frequency of BSSs with respect to HB stars for M53 (*upper panel*) and M3 (*lower panel*), plotted as a function of the distance from the cluster center in units of r_c . Vertical arrows mark the estimated position of the radius of avoidance of the two clusters (see text for details).

REFERENCES

- Beccari et al., 2008 in preparation
- Bedin, L. R., Cassisi, S., Castelli, F., Piotto, G., Anderson, J., Salaris, M., Momany, Y., & Pietrinferni, A. 2005, MNRAS, 357, 1038
- Bertin E., Arnouts S., 1996, A&AS, 117, 393
- Clement, C. M., et al. 2001, AJ, 122, 2587
- Combes, F., Leon, S., & Meylan, G. 1999, A&A, 352, 149
- Dalessandro, E., et al. 2008, in preparation
- Dalessandro, E., Lanzoni, B., Ferraro, F. R., Rood, R. T., Milone, A., Piotto, G., & Valenti, E. 2007, ArXiv e-prints, 712, arXiv:0712.4272
- De Marchi G., Paresce F., Portegies Zwart S., 2005, in Corbelli E., Palle F., eds, ASSL Vol. 327, The Initial Mass Function 50 Years Later. Springer-Verlag, Dordrecht, p. 77
- Ferraro, F. R., Pecci, F. F., Cacciari, C., Corsi, C., Buonanno, R., Fahlman, G. G., & Richer, H. B. 1993, AJ, 106, 2324
- Ferraro, F. R., et al. 1997, A&A, 324, 915
- Ferraro, F. R., Beccari, G., Rood, R. T., Bellazzini, M., Sills, A., & Sabbi, E. 2004, ApJ, 603, 127
- Ferraro, F. R., Sollima, A., Rood, R. T., Origlia, L., Pancino, E., & Bellazzini, M. 2006a, ApJ, 638, 433
- Ferraro, F. R., et al. 2006b, ApJ, 647, L53
- Giallongo, E., et al. 2008, ArXiv e-prints, 801, arXiv:0801.1474
- Hack W., Cox C., 2001, Instrum. Sci. Report, 2001-008
- Harris, W.E. 1996, AJ, 112, 1487
- Hill, J. M., Green, R. F., & Slagle, J. H. 2006, Proc. SPIE, 6267, 62670Y
- Jeon, Y.-B., Lee, M. G., Kim, S.-L., & Lee, H. 2003, AJ, 125, 3165
- Johnston, K. V., Sigurdsson, S., & Hernquist, L. 1999, MNRAS, 302, 771

- Lanzoni, B., Dalessandro, E., Perina, S., Ferraro, F. R., Rood, R. T., & Sollima, A. 2007, *ApJ*, 670, 1065 (L07a)
- Lanzoni, B., Dalessandro, E., Ferraro, F. R., Mancini, C., Beccari, G., Rood, R. T., Mapelli, M., & Sigurdsson, S. 2007b, *ApJ*, 663, 267
- Lanzoni, B., et al. 2007c, *ApJ*, 663, 1040
- Lehmann, I., & Scholz, R.-D. 1997, *A&A*, 320, 776
- Leon, S., Meylan, G., & Combes, F. 2000, *A&A*, 2000, 359, 907
- McLaughlin, D. E., & van der Marel, R. P. 2005, *ApJS*, 161, 304
- Mapelli, M., Sigurdsson, S., Ferraro, F. R., Colpi, M., Possenti, A., & Lanzoni, B. 2006, *MNRAS*, 373, 361
- Piotto, G., et al. 2002, *A&A*, 391, 945
- Ragazzoni, R., et al. 2006, *Proc. SPIE*, 6267, 626710
- Renzini, A., & Buzzoni, A. 1986, in *Spectral Evolution of Galaxies*, ed. C. Chiosi & A. Renzini (Dordrecht: Reidel), 135
- Rey, S.-C., Lee, Y.-W., Byun, Y.-I., & Chun, M.-S. 1998, *AJ*, 116, 1775 (R98)
- Robin A. C., Reil C., Derrire S., Picaud S., 2003, *A&A*, 409, 523
- Sabbi, E., Ferraro, F. R., Sills, A., & Rood, R. T. 2004, *ApJ*, 617, 1296
- Schechter, P. L., Mateo, M., & Saha, A. 1993, *PASP*, 105, 1342
- Sirianni et al., 2005, *PASP*, 117, 1049
- Sigurdsson, S., & Phinney, E. S. 1995, *ApJS*, 99, 609
- Sollima, A., Beccari, G., Ferraro, F. R., Fusi Pecci, F., & Sarajedini, A. 2007, *MNRAS*, 380, 781
- Stetson, P. B. 1987, *PASP*, 99, 191
- Stetson, P. B. 1994, *PASP*, 106, 250
- Trager, S. C., King, I. R., & Djorgovski, S. 1995, *AJ*, 109, 218
- Warren, S. R., Sandquist, E. L., & Bolte, M. 2006, *ApJ*, 648, 1026

Zaggia, S. R., Piotto, G., & Capaccioli, M. 1997, *A&A*, 327, 1004

Table 1: Photometric data.

Instrument	Filter	# of images	Exp Time [sec]
ACS	F606W	1	45
-	-	5	340
-	F814W	1	45
-	-	5	340
LBC-Blue	U	1	20
-	-	3	100
-	-	2	500
-	B	1	10
-	-	3	60
-	-	2	300
-	V	1	10
-	-	3	60
-	-	3	300
MEGACAM	g	2	90
-	r	2	180

Table 2: Number counts of BSSs and HB stars in the different data-sets.

Catalogue	# of BSSs	# of HBs
WFPC2/PC	36	65
ACS	73	296
LBC-Blue	69	175
MEGACAM	25	26

Table 3: Numbers and Specific Frequencies of BSS and HB stars for $r < 16.6'$.

r''	# of HBs	# of BSSs	N_{BSS}/N_{HB}	R_{BSS}	R_{HB}
0-20	73	37	0.51	1.65	1.11
20-36	76	30	0.39	1.15	1.00
36-55	75	14	0.19	0.52	0.96
55-79	79	11	0.14	0.47	1.16
79-130	72	24	0.34	0.94	0.96
130-230	78	26	0.34	0.99	1.02
230-1000	91	44	0.48	1.23	0.87

Table 4: Structural parameters of M3 and M53.

Cluster	r_c''	c	ρ_0 M_\odot/pc^3	r_{avoid}/r_c
M3	25	1.77	3.0×10^3	4.9
M53	25	1.60	2.2×10^3	4.5